

# Experimental Demonstration of Commutation Relations Using Intensity Correlations

Hans Dang,<sup>1,2</sup> Sebastian Luff,<sup>1,2</sup> Martin Fischer,<sup>2</sup> Markus Sondermann,<sup>1,2,3</sup>  
Mojdeh. S. Najafabadi,<sup>2</sup> Luis L. Sánchez-Soto,<sup>2,4,5</sup> and Gerd Leuchs<sup>1,2,6</sup>

<sup>1</sup>*Institut für Optik, Information und Photonik, Friedrich-Alexander-Universität Erlangen-Nürnberg, 91058 Erlangen, Germany*

<sup>2</sup>*Max-Planck-Institut für die Physik des Lichts, 91058 Erlangen, Germany*

<sup>3</sup>*Lehrstuhl für Experimentalphysik, Friedrich-Alexander-Universität Erlangen-Nürnberg, 91058 Erlangen, Germany*

<sup>4</sup>*Departamento de Óptica, Facultad de Física, Universidad Complutense, 28040 Madrid, Spain*

<sup>5</sup>*Institute for Quantum Studies, Chapman University, Orange, CA 92866, USA*

<sup>6</sup>*Department of Physics, University of Ottawa, Ottawa, Ontario K1N 6N5, Canada*

The canonical commutation relation is a cornerstone of quantum theory and underlies the Heisenberg uncertainty principle. Although uncertainty relations have been extensively tested, direct verifications of the underlying commutation relation itself have remained elusive. We report an experimental demonstration of the bosonic commutation relation for optical field operators based on measurements of two distinct intensity correlation functions. From these measurements, we extract the expectation value of the field-operator commutator for both a single-photon state and coherent state. In both cases, the measured values are consistent with unity, in quantitative agreement with quantum theory.

*Introduction.*—Heisenberg’s uncertainty principle, whether framed in terms of indeterminacy [1] or complementarity [2], is rooted in a fundamental feature of quantum mechanics: the noncommutativity of operators associated with complementary observables. In stark contrast to classical intuition, this principle asserts that certain pairs of physical properties, such as position and momentum or wavelike and particlelike behavior, cannot be simultaneously specified with arbitrary precision in the same experiment. This inherent uncertainty is not a limitation of measurement, but a fundamental property of nature itself.

Although the uncertainty principle has been rigorously tested across a wide range of physical systems, direct experimental access to the commutation relations that underpin it remains elusive. This difficulty arises because noncommuting observables do not admit a joint probability distribution, and their product is generally non-Hermitian, precluding straightforward measurement. To date, experimental demonstrations have been largely confined to finite-dimensional qubit systems [3–7]. In the continuous-variable domain, the canonical commutation relation between position and momentum—or, equivalently, between bosonic creation and annihilation operators—has been explored indirectly via sequential single-photon addition and subtraction from an optical field [8, 9].

We address this question from a different perspective by exploiting intensity correlation measurements, a technique pioneered by Hanbury Brown and Twiss (HBT) [10, 11] and formally grounded in Glauber’s quantum theory of optical coherence [12–14]. In a conventional HBT experiment, an optical field is incident on a 50:50 beam splitter, and the two output fields are detected by independent detectors whose signals are subsequently time-correlated. This approach enabled the landmark observation of photon antibunching [15–18], which is widely regarded as compelling experimental evidence for the particle nature of light [19].

The HBT arrangement has become the gold standard for measuring intensity correlation functions, yet it can misleadingly suggest that a beam splitter is essential to demonstrate

photon indivisibility. As pointed out by Loudon [20], a much simpler configuration, in which light is incident on a single-photon detector, is in principle sufficient. In such a simple scheme, correlations are extracted from the time-resolved detection record via auto-correlation analysis [21, 22]. While computationally efficient, this method yields a pronounced peak at zero time delay (as is to be expected for every auto-correlation function) that is absent in cross-detector measurements.

In this Letter, we demonstrate that the distinction between cross-correlation and auto-correlation measurements is not merely technical, but reflects a fundamental consequence of the noncommutativity of bosonic field operators. Specifically, HBT cross-correlations probe a normal ordering of field operators that is intrinsically different from the operator ordering accessed in single-detector auto-correlations. By quantitatively comparing these two classes of intensity correlations, we show that the zero-delay auto-correlation peak—commonly regarded as an artifact—constitutes a direct experimental manifestation of the bosonic commutation relation.

Moreover, we generalize this approach to establish a framework for determining commutation relations through intensity correlation measurements. Remarkably, our method applies to arbitrary optical fields and operates independently of whether their statistics are classical or quantum, underscoring both its fundamental significance and its broad experimental accessibility.

*Theoretical background.*—We consider the standard HBT setup. Within Glauber photodetection theory [13], the joint probability of detecting a photon at time  $t$  in one detector and another photon at time  $t'$  in the second detector is proportional to  $w(t, t') \propto \langle \hat{E}^{(-)}(t) \hat{E}^{(-)}(t+\tau) \hat{E}^{(+)}(t+\tau) \hat{E}^{(+)}(t) \rangle := G^{(2)}(t, t')$ , where  $\tau = t' - t$  is the time delay,  $\hat{E}^{(\pm)}$  are the positive (negative) parts of the fields and the angle brackets indicate ensemble averages evaluated with the use of the density matrix as  $\langle \hat{O} \rangle = \text{Tr}(\hat{\rho} \hat{O})$  for any observable  $\hat{O}$ . In what follows, we assume the fields to be ergodic, so that ensemble averages are equivalent to time averages [23].

This measurement thus yields the second-order correlation function

$$g_{\text{cross}}^{(2)}(\tau) = \frac{\langle :\hat{I}(t)\hat{I}(t+\tau): \rangle}{\langle :\hat{I}(t): \rangle^2} = \frac{\langle \hat{a}^\dagger(t)\hat{a}^\dagger(t+\tau)\hat{a}(t)\hat{a}(t+\tau) \rangle}{\langle \hat{a}^\dagger(t)\hat{a}(t) \rangle^2}, \quad (1)$$

where  $\hat{I}(t) = \hat{E}^{(-)}(t)\hat{E}^{(+)}(t)$  is the intensity operator and  $:\cdot:$  denotes normal ordering. The subscript “cross” stresses that we cross-correlate the signals measured with two different detectors, including the correlation at zero delay  $\tau = 0$ . For stationary fields, this definition is independent of the choice of the absolute detection time  $t$ .

A key feature of  $g_{\text{cross}}^{(2)}(\tau)$  is its independence from optical losses, which makes it particularly robust experimentally. This robustness, however, comes at the expense of reduced sensitivity to absolute photon-number statistics. In addition, the HBT configuration is unaffected by detector dead time. The above discussion applies to energy-detecting measurements, such as photodiodes or click detectors, but not to quadrature-sensitive detection schemes, e.g., homodyne detection [24–26].

Most intensity-correlation measurements employ the HBT scheme. One may nevertheless ask why the correlation function is not instead obtained by recording a time series with a single detector and evaluating the correlation numerically [22]. We denote the resulting auto-correlation function as  $g_{\text{auto}}^{(2)}$ . In contrast to the HBT cross-correlation  $g_{\text{cross}}^{(2)}$ ,  $g_{\text{auto}}^{(2)}$  is not generally independent of losses, a consequence of the nontrivial effect of attenuation on quantum signals. Importantly, however, losses affect only the zero-delay value: for all  $\tau \neq 0$ , the two correlation functions are identical.

This property can be of advantage in experiments. Instead of splitting the incoming light using a beam splitter onto two detectors and correlating the resulting two time series, it might be already sufficient to simply send all the light to a single detector with a fast response time, and calculate the auto-correlation function instead. Depending on the delay range of interest, this can significantly reduce the required measurement time. For example, sending  $N$  photons into an HBT setup with a beam splitter of reflectivity  $R$  and transmissivity  $1 - R$ , the expected number of correlations scales as  $N/R \times N/(1 - R) = N^2/(R - R^2)$ . In contrast, when the same photons are detected by a single detector and auto-correlated, the number of correlations at  $\tau \neq 0$  scales as  $N^2 - N$ . Hence, the number of data points contributing to  $g_{\text{cross}}^{(2)}(\tau)$  scales as  $\mathcal{O}(N^2/(R - R^2))$ , whereas for  $g_{\text{auto}}^{(2)}(\tau)$  it scales as  $\mathcal{O}(N^2)$ . For the optimal case of a 50:50 beam splitter, this translates to a reduction in the required measurement time by a factor of four.

The two approaches differ, however, at zero delay. The discrepancy arises because  $g_{\text{cross}}^{(2)}(0)$  involves the product of two independent signals measured by different detectors, whereas  $g_{\text{auto}}^{(2)}(0)$  corresponds to correlating a signal with itself. For attenuated fields, these operations are not equivalent due to the projection associated with quantum measurement [27]. In particular, attenuating a train of single-photon pulses does not result in uniformly reduced pulse amplitudes; instead, some pulses are removed entirely while others remain unchanged.

A photon thus appears in a given time bin only with a small probability, but when it does, it is detected as a full photon. Auto-correlating such a signal therefore assigns unit conditional detection probability to a second photon at  $\tau = 0$ , rather than a reduced probability reflecting optical losses.

Quantum theory captures this effect nicely. Recording a single intensity time series and correlating it with itself—typically averaging over time—leads to the auto-correlation function

$$g_{\text{auto}}^{(2)}(0) = \frac{\langle \hat{I}^2(t) \rangle}{\langle \hat{I}(t) \rangle^2} = \frac{\langle \hat{a}^\dagger(t)\hat{a}(t)\hat{a}^\dagger(t)\hat{a}(t) \rangle}{\langle \hat{a}^\dagger(t)\hat{a}(t) \rangle^2} \quad (2)$$

A simple but crucial observation is that, for a pure quantum state  $|\psi\rangle$ , the difference between the auto- and cross-correlation functions at zero delay is given by

$$g_{\text{auto}}^{(2)}(0) - g_{\text{cross}}^{(2)}(0) = \frac{\langle \phi | [\hat{a}(t), \hat{a}^\dagger(t)] | \phi \rangle}{\langle \hat{a}^\dagger(t)\hat{a}(t) \rangle}, \quad (3)$$

where  $|\phi\rangle = 1/\sqrt{\langle \hat{a}^\dagger \hat{a} \rangle} \hat{a}|\psi\rangle$  is the state of the field immediately after a photon has been detected. Thus, the difference  $g_{\text{auto}}^{(2)}(0) - g_{\text{cross}}^{(2)}(0)$  provides direct access to the bosonic commutation relations. In what follows, we exploit this relation to test these fundamental quantum properties.

*Auto- vs cross-correlation at zero delay.*— To experimentally assess the difference  $g_{\text{auto}}^{(2)}(0) - g_{\text{cross}}^{(2)}(0)$  we begin by using the commutator for the field operators. After integrating over time, this yields

$$g_{\text{auto}}^{(2)}(0) - g_{\text{cross}}^{(2)}(0) = \frac{1}{\langle \hat{a}^\dagger(t)\hat{a}(t) \rangle}, \quad (4)$$

In a realistic experimental setting, however, the number of detected photons  $N_{\text{det}}(t)$  generally differs from the ideal mean photon number  $\langle \hat{a}^\dagger(t)\hat{a}(t) \rangle$ . Their relation can be written as

$$N_{\text{det}}(t) = \frac{\min\{A_{\text{det}}, A_{\text{mode}}\}}{A_{\text{mode}}} \frac{T_{\text{bw}}}{T_{\text{coh}}} \eta \langle \hat{a}^\dagger(t)\hat{a}(t) \rangle. \quad (5)$$

This expression contains three multiplicative factors that account for experimental imperfections. The first factor describes the spatial overlap between the optical mode and the detector: if the mode cross-section  $A_{\text{mode}}$  is larger than the photosensitive area of the detector  $A_{\text{det}}$  some signal will be lost, resulting in losses.

The second factor accounts for temporal overlap. When the coherence time  $T_{\text{coh}}$  exceeds the measurement time interval  $T_{\text{bw}}$ , the signal per bin is also reduced; conversely, it is enhanced when  $T_{\text{coh}} < T_{\text{bw}}$ .

Finally, the efficiency factor  $\eta$  captures all optical losses, including the non-unit quantum efficiency of the detector. These losses are commonly modeled by introducing a fictitious beam splitter with transmission  $\eta$  in front of an ideal detector, such that only a fraction  $\eta$  of the incident photons reach the detector while the remainder are lost into an unobserved vacuum mode [28].

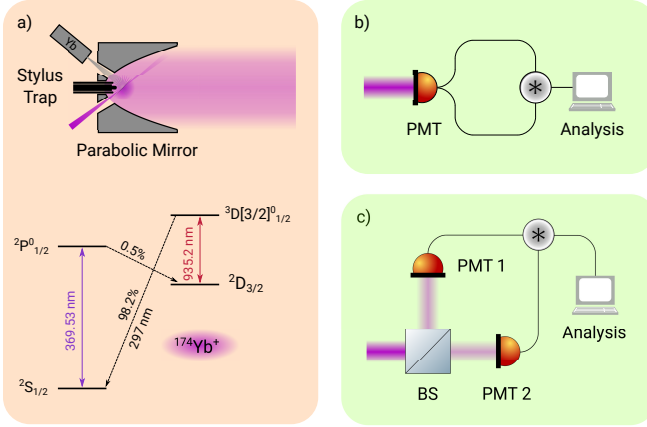


FIG. 1. a) Sketch of the parabolic mirror with inserted trap assembly and  $^{174}\text{Yb}^+$  energy levels. The light scattered towards the detection setup is either emitted by the ion at the focus of the parabolic mirror (ion-focus distance not to scale) or laser light scattered from one of the trap electrodes. b) and c) Sketches of the used detection methods.

As a result, the difference between  $g_{\text{auto}}^{(2)}$  and  $g_{\text{cross}}^{(2)}$  is given by

$$g_{\text{auto}}^{(2)}(0) - g_{\text{cross}}^{(2)}(0) = \frac{1}{\min\{A_{\text{det}}, A_{\text{mode}}\} \frac{T_{\text{bw}}}{T_{\text{coh}}} \eta \langle \hat{a}^\dagger(t) \hat{a}(t) \rangle}.$$
(6)

*Experimental results.*— In the following we illustrate how these considerations translate into two different experimental scenarios. In each experiment, we independently measure  $g_{\text{auto}}^{(2)}(0)$  and  $g_{\text{cross}}^{(2)}(0)$  and subsequently apply Eq. (3). Care must be taken, however, to properly account for optical losses and the finite measurement time window, as both affect the experimentally observed correlation functions.

In the first experiment, which serves as an example of a single-photon source, we employ a single  $^{174}\text{Yb}^+$  ion trapped at the focus of a deep parabolic mirror, similar to the setup in Ref. [29]. Fluorescence emitted by the ion is collimated by the parabolic mirror, and straylight is suppressed by a pinhole in the Fourier plane of a telescope. The collected light is then divided by a 50:50 beam splitter and directed onto two photomultiplier tubes (PMTs), whose detection events are recorded with a time-to-digital converter and analyzed numerically (see Fig. 1).

The ion is continuously illuminated using a 369.5 nm laser driving the  $^2\text{S}_{1/2} - ^2\text{P}_{1/2}$  dipole transition, which has a linewidth of  $\Gamma = 2\pi \times 19.6$  MHz given by the lifetime of 8.1 ns of the  $^2\text{P}_{1/2}$  state [30]. The single photons emitted by the ion during this process are then used for the correlation measurements. A repump laser at 935 nm prevents population trapping in the  $^2\text{D}_{3/2}$  state, which arises with branching ratio of  $1 - \beta = 0.005$  from the  $^2\text{P}_{1/2}$ , thereby closing the cooling cycle.

The  $^2\text{S}_{1/2} - ^2\text{P}_{1/2}$  transition was driven at a saturation parameter of  $S = 1.00 \pm 0.11$  (determined separately from saturation measurements) and a detuning of  $-\Gamma/2$ , corresponding to

an upper-state population of  $\rho_{22} = S/[2(1+S)] = 0.25 \pm 0.01$ . From these parameters, the expected fluorescence rate is  $R_{\text{sc}} = \beta \Gamma \rho_{22} = \beta \rho_{22} / T_{\text{coh}}$ . For  $S = 1$ , the expected scattering rate is approximately  $R_{\text{sc}} \simeq 30.7 \times 10^6$  photons per second. Experimentally, however, the combined count rate on both detectors was  $\sim 1.40 \pm 0.01$  Mega counts per second, corresponding to a first-estimate detection efficiency of  $4.56 \pm 0.04$  %.

A more accurate determination of  $\eta$  was obtained via a state-sensitive method. The ion was first Doppler cooled and prepared in the  $^2\text{S}_{1/2}$  ground state. Continuous 369.5 nm laser light then excited the ion to the  $^2\text{P}_{1/2}$  state via the  $^2\text{S}_{1/2} - ^2\text{P}_{1/2}$  dipole transition. From the excited state, the ion either decays back to the ground state with probability  $\beta$ , emitting a photon, or to the metastable  $^2\text{D}_{3/2}$  state with probability of  $1 - \beta$ . In the former case, the laser re-excites the ion, and this cycle repeats, producing one photon per cycle until the ion eventually decays to the metastable state. The probability for the ion to emit  $n$  photons is therefore  $P_{\text{sc}}(n) = \beta^n (1 - \beta)$ . Accounting for the overall detection efficiency  $\eta$ , the probability to detect  $k$  photons is

$$P_{\text{det}}(k) = \sum_{n=k}^{\infty} \binom{n}{k} \eta^k (1 - \eta)^{n-k} P_{\text{scat}}(n) = \frac{(1 - \beta) \beta^k \eta^k}{(1 + \beta(\eta - 1))^{(k+1)}}.$$
(7)

By repeatedly preparing the ion in the ground state and recording the number of emitted photons until decay to the metastable state,  $\eta$  can be extracted by fitting Eq. (7) to the observed photon-number distribution.

Using this method, the detection efficiency was measured to be  $1.94 \pm 0.02$  % for the detector in transmission and  $2.67 \pm 0.02$  % for the detector in reflection. This results in an overall detection efficiency of  $\eta = 4.61 \pm 0.03$  % for the combined detectors in our setup.

The same time-tag streams from both detectors were used to evaluate  $g_{\text{auto}}^{(2)}(0)$  and  $g_{\text{cross}}^{(2)}(0)$ . For  $g_{\text{auto}}^{(2)}(0)$ , the “single detector” was realized by first merging the two time-tag streams into a single stream and then correlating it with itself (see Fig. 1b)). By merging the two streams, detector-specific artifacts such as photomultiplier dead time are effectively suppressed. The cross-correlation  $g_{\text{cross}}^{(2)}(0)$  was obtained by correlating the time-tag stream from one detector with that of the other (see Fig. 1c)). In both cases, correlations were calculated by counting coincidence events at time delays  $\tau$  within a time window of  $T_{\text{bw}}$ , followed by appropriate normalization.

The resulting correlation functions for a train of single photons emitted by a single ion are shown in Fig. 2, evaluated with a binwidth of  $T_{\text{bw}} = 1$  ns. Both correlation functions are nearly identical, except at zero delay, in agreement with our theoretical prediction. The pronounced antibunching dip is clearly visible, confirming the single-photon character of the source. We obtain  $g_{\text{auto}}^{(2)}(0) = 714.93 \pm 0.19$  and  $g_{\text{cross}}^{(2)}(0) = 0.016 \pm 0.002$ . In the ideal limit of vanishing straylight,  $g_{\text{cross}}^{(2)}(0)$  should be zero for a single-photon source.

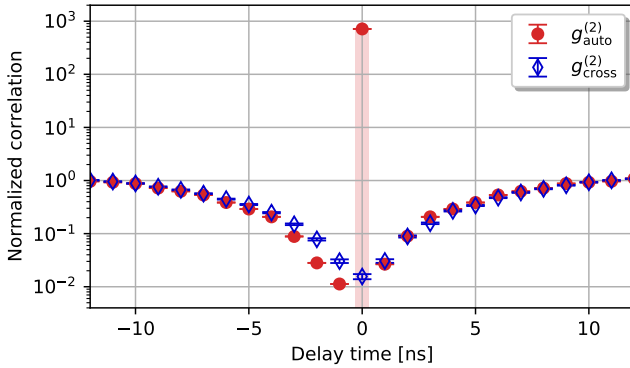


FIG. 2. Measured correlation functions  $g_{\text{auto}}^{(2)}$  and  $g_{\text{cross}}^{(2)}$  of a train of single photons emitted by a single trapped ion. Both functions are nearly identical and only differ for  $\tau = 0$ , as expected from theory. The characteristic antibunching dip for a single-photon source is also apparent from the correlation functions.

On average, the ion emits  $\beta\rho_{22}$  photons per excited-state lifetime on the  $^2\text{S}_{1/2} - ^2\text{P}_{1/2}$  transition, of which only a fraction  $\eta$  are detected within the measurement time window  $T_{\text{bw}}$ . The mean number of detected photons within the measurement time window is thus given by  $\langle \hat{N} \rangle = \beta\rho_{22}\eta T_{\text{bw}}/T_{\text{coh}} = (1.42 \pm 0.01) \times 10^{-3}$  resulting in a value for the commutator, according to Eq. (3), of  $\langle \phi | [\hat{a}, \hat{a}^\dagger] | \phi \rangle = 1.01 \pm 0.04$ , which agrees very well with the expected value of one based on theory.

Our second experiment employs coherent states as the light source. The experimental setup and data analysis are, in principle, identical to those used for the single-photon source. In this case, the light source is a frequency- and power-stabilized 369.5 nm laser. It is referenced to an ultra-stable cavity, yielding a laser linewidth  $1/T_{\text{coh}}$  of approximately 10 Hz. Light from the laser is scattered off the ion-trap assembly into the detection path, where the corresponding correlation functions are recorded. The resulting measurements are shown in Fig. 3.

Both the PMTs and the time-to-digital converter have finite dead times of 1.5 ns and 2 ns, respectively. This instrumental limitation produces the dip observed in  $g_{\text{auto}}^{(2)}(0)$  at zero delay. In contrast, the cross-correlation is unaffected, as it involves two independent detectors. Aside from this effect,  $g_{\text{auto}}^{(2)}(0)$  and  $g_{\text{cross}}^{(2)}(0)$  are flat and equal to unity, as expected for a coherent source, except for the auto-correlation peak at  $\tau = 0$ .

For  $\tau \neq 0$ , a straightforward extension of the arguments leading to (3) yields

$$g_{\text{auto}}^{(2)}(\tau) - g_{\text{cross}}^{(2)}(\tau) = \frac{\langle \phi(t) | [\hat{a}(t), \hat{a}^\dagger(t')] | \phi(t') \rangle}{\sqrt{\langle \hat{a}^\dagger(t)\hat{a}(t) \rangle \langle \hat{a}^\dagger(t')\hat{a}(t') \rangle}}. \quad (8)$$

From the experimental results we therefore conclude that  $[\hat{a}(t), \hat{a}^\dagger(t')] = \delta(t - t')$ , implying that the field operators commute at different times.

The average number of detected photon counts per binwidth  $T_{\text{bw}} = 1$  ns is measured to be  $\langle N \rangle = (1.19 \pm 0.01) \cdot 10^{-3}$ , as extracted from the mean count rate of the detectors. Losses in the detection setup are already accounted for when using

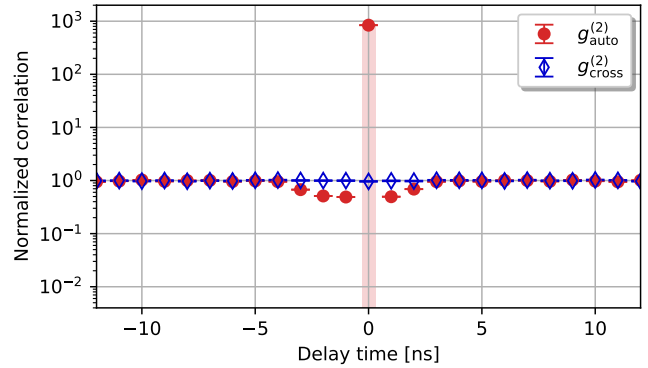


FIG. 3. Measured correlation functions  $g_{\text{auto}}^{(2)}$  and  $g_{\text{cross}}^{(2)}$  of coherent laser light. The dip in the auto-correlation function for values close to  $\tau = 0$  is caused by the pulse width of 1.5 ns of the detectors and the dead time of 2 ns of the time-to-digital converter used to record the signals. Aside from the dip and the auto-correlation peak, both functions show a constant value of one, as expected for a coherent source.

the detected count rate to calculate the mean photon number. For the auto-correlation, we find  $g_{\text{auto}}^{(2)}(0) = 841.68 \pm 0.24$ , which is in good agreement with the expectation of  $g_{\text{auto}}^{(2)}(0) = 1 + 1/\langle N \rangle$  for a coherent state. For the cross-correlation, we find a value of  $g_{\text{cross}}^{(2)}(0) = 0.97 \pm 0.02$  close to one, as expected for a coherent source. Calculating the commutator using these values then yields  $\langle \phi | [\hat{a}, \hat{a}^\dagger] | \phi \rangle = 1.00 \pm 0.02$ , which is again consistent with the theoretically expected value of one.

*Concluding remarks.*— We emphasize that the auto- and cross-correlation functions of the light intensity—and in particular their difference at zero time delay—contain useful information that is often overlooked. For instance, this difference can be used to characterize parameters with potentially reduced uncertainties, as discussed elsewhere. Here, we focused on the remarkable fact that the difference between the correlation functions at zero delay is directly proportional to the commutator of the quantum-mechanical creation and annihilation operators.

Experimentally, we confirmed the noncommutativity of these operators by measuring both the normalized auto- and cross-correlation functions for two fundamentally different light sources: a single-photon source and a coherent source. In both cases, the light was split by a beam splitter onto two detectors. The cross-correlation was obtained by correlating the independent detector time series, while for the auto-correlation, the two time series were first merged before correlating the resulting stream with itself. Using the same underlying data set for both correlations, we calculated the difference between the normally ordered cross-correlation and the not normally-ordered auto-correlation, and multiplied by the mean photon number. This procedure yielded a commutator value close to unity for both sources, in excellent agreement with theoretical expectations.

*Acknowledgments.*— We acknowledge discussions with A. Z. Goldberg. L. L. S.-S. was supported by the Spanish Agencia Estatal de Investigación (Grant PID2021-127781NB-I00).

- 
- [1] W. Heisenberg, *Z. Phys.* **43**, 172 (1927).
- [2] N. Bohr, *Nature* **121**, 580 (1928).
- [3] Y. Hasegawa, S. Menhart, R. Meixner, and G. Badurek, *Phys. Lett. A* **234**, 322 (1997).
- [4] A. G. Wagh, V. C. Rakhecha, J. Summhammer, G. Badurek, H. Weinfurter, B. E. Allman, H. Kaiser, K. Hamacher, D. L. Jacobson, and S. A. Werner, *Phys. Rev. Lett.* **78**, 755 (1997).
- [5] Y.-S. Kim, H.-T. Lim, Y.-S. Ra, and Y.-H. Kim, *Phys. Lett. A* **374**, 4393 (2010).
- [6] X.-C. Yao, J. Fiurášek, H. Lu, W.-B. Gao, Y.-A. Chen, Z.-B. Chen, and J.-W. Pan, *Phys. Rev. Lett.* **105**, 120402 (2010).
- [7] R. Wagner, W. Kersten, A. Danner, H. Lemmel, A. K. Pan, and S. Sponar, *Phys. Rev. Res.* **3**, 023243 (2021).
- [8] A. Zavatta, S. Viciani, and M. Bellini, *Science* **306**, 660 (2004).
- [9] A. Zavatta, V. Parigi, M. S. Kim, H. Jeong, and M. Bellini, *Phys. Rev. Lett.* **103**, 140406 (2009).
- [10] R. H. Brown and R. Q. Twiss, *Nature* **177**, 27 (1956).
- [11] R. Hanbury Brown and R. Q. Twiss, *Nature* **178**, 1046 (1956).
- [12] R. J. Glauber, *Phys. Rev. Lett.* **10**, 84 (1963).
- [13] R. J. Glauber, *Phys. Rev.* **130**, 2529 (1963).
- [14] R. J. Glauber, *Phys. Rev.* **131**, 2766 (1963).
- [15] H. J. Kimble, M. Dagenais, and L. Mandel, *Phys. Rev. Lett.* **39**, 691 (1977).
- [16] J. D. Cresser, J. Häger, G. Leuchs, M. Rateike, and H. Walther, “Resonance fluorescence of atoms in strong monochromatic laser fields,” in *Dissipative Systems in Quantum Optics: Resonance Fluorescence, Optical Bistability, Superfluorescence*, edited by R. Bonifacio (Springer, Berlin, 1982) pp. 21–59.
- [17] D. F. Walls, *Nature* **280**, 451 (1979).
- [18] G. Leuchs, “Photon statistics, antibunching and squeezed states,” in *Frontiers of nonequilibrium statistical physics*, edited by G. T. Moore and M. O. Scully (Springer, New York, 1986) pp. 329–360.
- [19] P. Grangier, G. Roger, and A. Aspect, *EPL* **1**, 173 (1986).
- [20] R. Loudon, *The Quantum Theory of Light* (Oxford University Press, Oxford, 1973).
- [21] J. Wiersig, C. Gies, F. Jahnke, M. Aßmann, T. Berstermann, M. Bayer, C. Kistner, S. Reitzenstein, C. Schneider, S. Höfling, *et al.*, *Nature* **460**, 245 (2009).
- [22] G. A. Steudle, S. Schietinger, D. Höckel, S. N. Dorenbos, I. E. Zadeh, V. Zwiller, and O. Benson, *Phys. Rev. A* **86**, 053814 (2012).
- [23] L. Mandel and E. Wolf, *Optical Coherence and Quantum Optics* (Cambridge University Press, 1995) pp. 473–476.
- [24] G. Björk, P. Jonsson, and L. L. Sánchez-Soto, *Phys. Rev. A* **64**, 042106 (2001).
- [25] B. Hessmo, P. Usachev, H. Heydari, and G. Björk, *Phys. Rev. Lett.* **92**, 180401 (2004).
- [26] M. Shikhali Najafabadi, L. L. Sanchez-Soto, K. Huang, J. Laurat, H. Le Jeannic, and G. Leuchs, *Phil. Trans. R. Soc. A* **382**, 20230337 (2024).
- [27] I. Khan, D. Elser, T. Dirmeier, C. Marquardt, and G. Leuchs, *Phil. Trans. R. Soc. A* **375**, 20160235 (2017).
- [28] A. Meda, E. Losero, N. Samantaray, F. Scafirimuto, S. Pradyumna, I. Avella, A. Ruo-Berchera, and M. Genovese, *J. Opt.* **19**, 094002 (2017).
- [29] R. Maiwald, A. Golla, M. Fischer, M. Bader, S. Heugel, B. Chalopin, M. Sondermann, and G. Leuchs, *Phys. Rev. A* **86**, 043431 (2012).
- [30] R. W. Berends, E. H. Pinnington, B. Guo, and Q. Ji, *J. Phys. B: Atom. Mol. Opt. Phys.* **J** **26**, L701 (1993).